Vol 460|20 August 2009|doi:10.1038/nature08236

LETTERS

Neurotransmission selectively regulates synapse formation in parallel circuits *in vivo*

Daniel Kerschensteiner[1,2]†, Josh L. Morgan[1,2], Edward D. Parker[3], Renate M. Lewis[1] & Rachel O. L. Wong[1,2]

Activity is thought to guide the patterning of synaptic connections in the developing nervous system. Specifically, differences in the activity of converging inputs are thought to cause the elimination of synapses from less active inputs and increase connectivity with more active inputs[1,2]. Here we present findings that challenge the generality of this notion and offer a new view of the role of activity in synapse development. To imbalance neurotransmission from different sets of inputs *in vivo*, we generated transgenic mice in which ON but not OFF types of bipolar cells in the retina express tetanus toxin (TeNT). During development, retinal ganglion cells (RGCs) select between ON and OFF bipolar cell inputs (ON or OFF RGCs) or establish a similar number of synapses with both on separate dendritic arborizations (ON-OFF RGCs). In TeNT retinas, ON RGCs correctly selected the silenced ON bipolar cell inputs over the transmitting OFF bipolar cells, but were connected with them through fewer synapses at maturity. Time-lapse imaging revealed that this was caused by a reduced rate of synapse formation rather than an increase in synapse elimination. Similarly, TeNT-expressing ON bipolar cell axons generated fewer presynaptic active zones. The remaining active zones often recruited multiple, instead of single, synaptic ribbons. ON-OFF RGCs in TeNT mice maintained convergence of ON and OFF bipolar cells inputs and had fewer synapses on their ON arbor without changes to OFF arbor synapses. Our results reveal an unexpected and remarkably selective role for activity in circuit development *in vivo*, regulating synapse formation but not elimination, affecting synapse number but not dendritic or axonal patterning, and mediating independently the refinement of connections from parallel (ON and OFF) processing streams even where they converge onto the same postsynaptic cell.

ON bipolar cells, which depolarize in response to light, receive and invert photoreceptor signals through metabotropic glutamate receptors (mGluR6) on their dendrites. OFF bipolar cells, on the other hand, express ionotropic glutamate receptors and hyperpolarize upon illumination[3,4]. Thus, the parallel processing of light increment (ON) and decrement (OFF) signals that is central to visual system function is initiated at the first synapse in the retina. To create an imbalance of glutamate release from ON and OFF bipolar cells in the inner plexiform layer where their axons relay signals to RGCs, we generated transgenic mice in which a promoter fragment of mGluR6 (ref. 5) drove expression of the light chain of TeNT and yellow fluorescent protein (*mGluR6-YFP/TeNT*, Fig. 1a). TeNT, a bacterial protease, cleaves vesicle-associated membrane protein 2 (VAMP2) and inhibits vesicle fusion[6]. In *mGluR6-YFP/TeNT* mice, transgene expression was limited to ON bipolar cells which ramify their axons in the inner half of the inner plexiform layer (Fig. 1b), and was present throughout the period of bipolar cell–RGC synaptogenesis (Supplementary Fig. 1). We tested the proteolytic activity of TeNT using an antibody against VAMP2 (ref. 7). Double-labelling for the vesicular glutamate transporter 1 (VGluT1), which is present in all bipolar cell axon terminals, verified that VAMP2 was selectively depleted from ON bipolar cells (Fig. 1c–h). To examine glutamate release, we recorded spontaneous excitatory postsynaptic currents (sEPSCs) from large monostratified RGCs in retinal flat mount preparations (Fig. 1i). ON RGCs from *mGluR6-YFP/TeNT* mice showed very few and lower amplitude sEPSCs compared to wild type, whereas OFF RGC sEPSCs were normal in frequency and amplitude (Fig. 1i–k). Focal application of the glutamate receptor agonist kainate (100 μM) near the soma of ON RGCs elicited excitatory currents of similar amplitude and without failure in wild-type and *mGluR6-YFP/TeNT* mice (Supplementary Fig. 2), showing that the reduction in spontaneous events probably reflects a blockade of presynaptic transmitter release.

To examine ON and OFF responses, which are driven by glutamate release from bipolar cells, we used multi-electrode arrays to record from ensembles of RGCs in wild-type and *mGluR6-YFP/TeNT* mice during visual stimulation. Receptive fields were characterized by the spike-triggered average (STA) stimulus during white noise presentation[8]. In wild-type retinas, all RGCs were light responsive, and ON and OFF RGCs displayed similar receptive field size and sensitivity (Fig. 1l–o). By contrast, in *mGluR6-YFP/TeNT* mice OFF RGCs showed normal receptive field properties, but ON responses were greatly reduced or absent (Fig. 1l–o). Taken together, these results suggest that in *mGluR6-YFP/TeNT* mice both spontaneous and evoked glutamate release were diminished from ON but not OFF bipolar cells.

Early in development, monostratified RGCs elaborate dendrites throughout the depth of the inner plexiform layer[9,10] and appear to be contacted by ON and OFF bipolar cells[11]. With maturation, dendritic branches are pruned and a single narrowly stratified arborization connected to either ON or OFF bipolar cells is maintained[12]. To visualize dendrites and excitatory synapses, we biolistically labelled single RGCs with tdTomato (tandem dimer Tomato) and PSD95–CFP (postsynaptic density protein 95–cyan fluorescent protein)[13]. Figure 2 shows that, despite the selective reduction of input activity from ON bipolar cells in *mGluR6-YFP/TeNT* mice, ON RGC dendrites stratified normally and their lateral branching patterns were indistinguishable from wild-type littermates (Fig. 2a, b, e and f and Supplementary Fig. 3). Excitatory postsynaptic sites marked by PSD95–CFP were localized precisely to appositions on ON RGC dendrites with TeNT-expressing ON bipolar cells (Fig. 2c, Supplementary Fig. 4 and Supplementary Movie 1), but were reduced in density by ~50% compared to wild type at postnatal day 21 (Fig. 2d, g and h). The remaining synapses showed similar centroperipheral distributions across dendritic fields as in wild type (Fig. 2d, i and j). These results indicate that input selection and dendritic stratification of postsynaptic RGCs in mice occur independently of bipolar cell activity

[1]Department of Anatomy and Neurobiology, Washington University School of Medicine, St Louis, Missouri 63110, USA. [2]Department of Biological Structure, [3]Department of Ophthalmology, University of Washington, Seattle, Washington 98195, USA.
†Present Address: Department of Ophthalmology and Visual Sciences, Washington University School of Medicine, St Louis, Missouri 63110, USA.

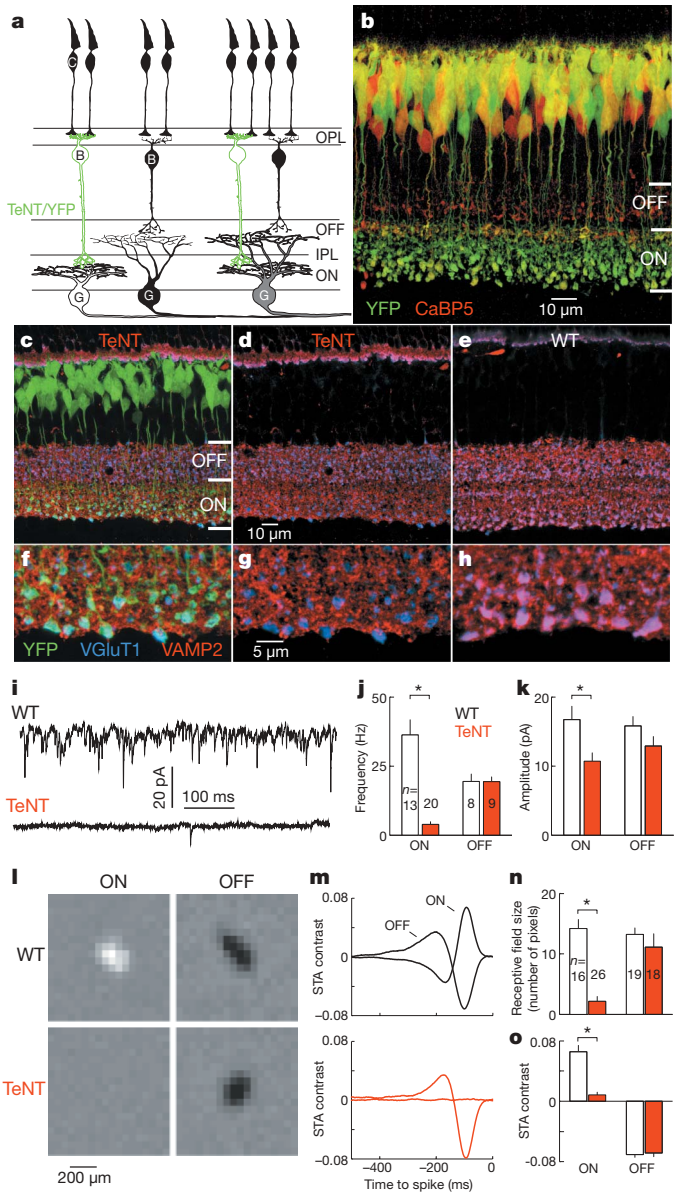

Figure 1 | Selective blockade of glutamate release from retinal ON bipolar cells. a, ON and OFF pathways. B, bipolar cell; C, cone; G, ganglion cell; IPL, inner plexiform layer; OPL, outer plexiform layer. ON (white), OFF (black) and ON-OFF responsiveness (grey) indicated by fill colour. **b**, YFP expression in *mGluR6-YFP/TeNT* mouse at postnatal day 21 colocalizes with anti-CaBP5 labelling in ON but not OFF bipolar cells[15]. **c–h**, Overview (**c–e**) and enlargements of ON sublamina (**f–h**) from postnatal day 21 *mGluR6-YFP/TeNT* (**c**, **d**, **f**, **g**) and wild-type (WT) retinas (**e**, **h**). YFP not shown in **d** and **g**. **i–k**, Representative traces (**i**, ON RGCs) and population data (mean + s.e.m., **j**, **k**) for sEPSCs recorded from RGCs at postnatal day 21. **l**, **m**, Spatial profile (**l**, 100 ms before spike) and time course (**m**, average of ten pixels with highest s.d.) of STAs from representative RGCs. **n**, **o**, Summary data (mean + s.e.m.) of receptive field extent (**n**, number of pixels with an s.d. that exceeded that of background pixels more than fourfold) and sensitivity (**o**, peak of average STA time course exemplified in **m**). Asterisk indicates $P < 0.01$.

(see Supplementary Information). Neurotransmission, however, is crucial for normal synaptic connectivity with the selected inputs.

In contrast to monostratified RGCs, bistratified RGCs maintain two narrowly stratified arborizations at distinct depths of the inner plexiform layer (Fig. 2k). The inner arbor is contacted by ON bipolar cells, the outer by OFF bipolar cells[3,4]. In wild-type mice, synaptic densities across both arborizations are correlated ($r = 0.86$; $P < 0.01$, $n = 8$ cells), presumably to balance ON and OFF light responses for each cell. If this balance was achieved by matching ON and OFF input activity, one would predict that a lower density of synapses on the ON arbor of bistratified RGCs in *mGluR6-YFP/TeNT* mice would be accompanied by a decrease in synapses on its OFF arbor. Alternatively, if ON and OFF bipolar cells engaged in synaptic competition, one might expect the density of OFF arbor synapses to increase[1,2]. Instead, we found that synaptic densities on the ON dendrites of bistratified RGCs were reduced ($P < 0.04$) without changes to OFF dendrites ($P > 0.4$, Fig. 2k–p). These results show that synaptic connections on the two arborizations are established independently of each other and are sensitive to transmitter release locally, but not to differences between inputs onto separate arbors of the same cell.

Several presynaptic changes could accompany the reduced density of synapses on RGC dendrites in *mGluR6-YFP/TeNT* mice: (1) there could be fewer ON bipolar cells; (2) their axonal arborizations could be smaller and less complex; and (3) the density of synapses along axonal arborizations could be reduced. Comparison with *mGluR6-GFP* mice[14] showed that the density of ON bipolar cells in *mGluR6-YFP/TeNT* mice was unchanged (*mGluR6-YFP/TeNT*, 32,045 ± 1,173 cells mm^{-2}; *mGluR6-GFP*, 30,820 ± 610 cells mm^{-2}; $P > 0.3$, Supplementary Fig. 5). To assess the structure of single bipolar cell axons, we generated *mGluR6-tdTomato* mice, selected founders in which isolated ON bipolar cells were labelled and crossed them to *mGluR6-YFP/TeNT* mice. Most of the tdTomato-expressing bipolar cells were type 6 and type 7 ON cone bipolar cells or rod bipolar cells (Supplementary Fig. 6)[15]. Axonal arborizations of these cell types retained their characteristic stratification and branching patterns in *mGluR6-YFP/TeNT* compared to wild-type background (Fig. 3a–f). However, when we labelled presynaptic sites in bipolar cell axons with an antibody against C-terminal binding protein 2 (CtBP2), we found that their density in *mGluR6-YFP/TeNT* mice was reduced (Fig. 3g and h).

To determine whether the remaining synapses were structurally normal, we obtained electron micrographs from retinas of *mGluR6-YFP/TeNT* mice and wild-type littermates. Vesicles at bipolar cell active zones are tethered to synaptic ribbons, a common feature of neurons using graded voltage signals rather than action potentials[16]. Each bipolar cell synapse normally contains a single ribbon, but the signals that regulate ribbon localization and number remain unknown[16]. As expected, all bipolar cell active zones (25 of 25) in wild-type mice contained single ribbons (Fig. 3i, j and Supplementary Figs 7 and 8). By contrast, at about half of the ON bipolar cell active zones (12 of 25) in *mGluR6-YFP/TeNT* mice, we found more than one and up to four ribbons (Fig. 3i, j). This phenotype was restricted to ON bipolar cells; only single ribbons (11 of 11) were found in the OFF sublamina of *mGluR6-YFP/TeNT* mice (Supplementary Fig. 7). Because active zones and ribbons assemble by insertion of Piccolo–Bassoon transport vesicles and/or the arrival of precursor spheres, both of which do not contain VAMP2[17,18], it seems unlikely that TeNT interferes directly with this process. Instead, we propose that transmitter release normally elicits a signal that prohibits the placement of further ribbons at this active zone (see Supplementary Information).

Because the number of bipolar cells, their axons and the RGC dendrites they contact were normal in TeNT retinas, it remained unclear which developmental mechanisms account for the lower density of bipolar cell–RGC synapses observed at maturity (Fig. 2). To begin to address this question, we measured the number and density of excitatory synapses on ON RGC dendrites at different times during development (Fig. 4a, b). At postnatal day 7, when synaptic transmission between bipolar cells and RGCs is first observed[19], synapse numbers and densities were indistinguishable between wild-type and *mGluR6-YFP/TeNT* mice ($P > 0.4$) and gradually diverged over the following days towards the differences observed at maturity (Fig. 4a, b). To assess the dynamics that underlie this divergent development, we carried out live imaging experiments of RGCs biolistically labelled with tdTomato and PSD95–CFP in *mGluR6-YFP/TeNT* mice and wild-type littermates at postnatal day 9 (refs 20, 21). Time-lapse imaging revealed frequent synapse

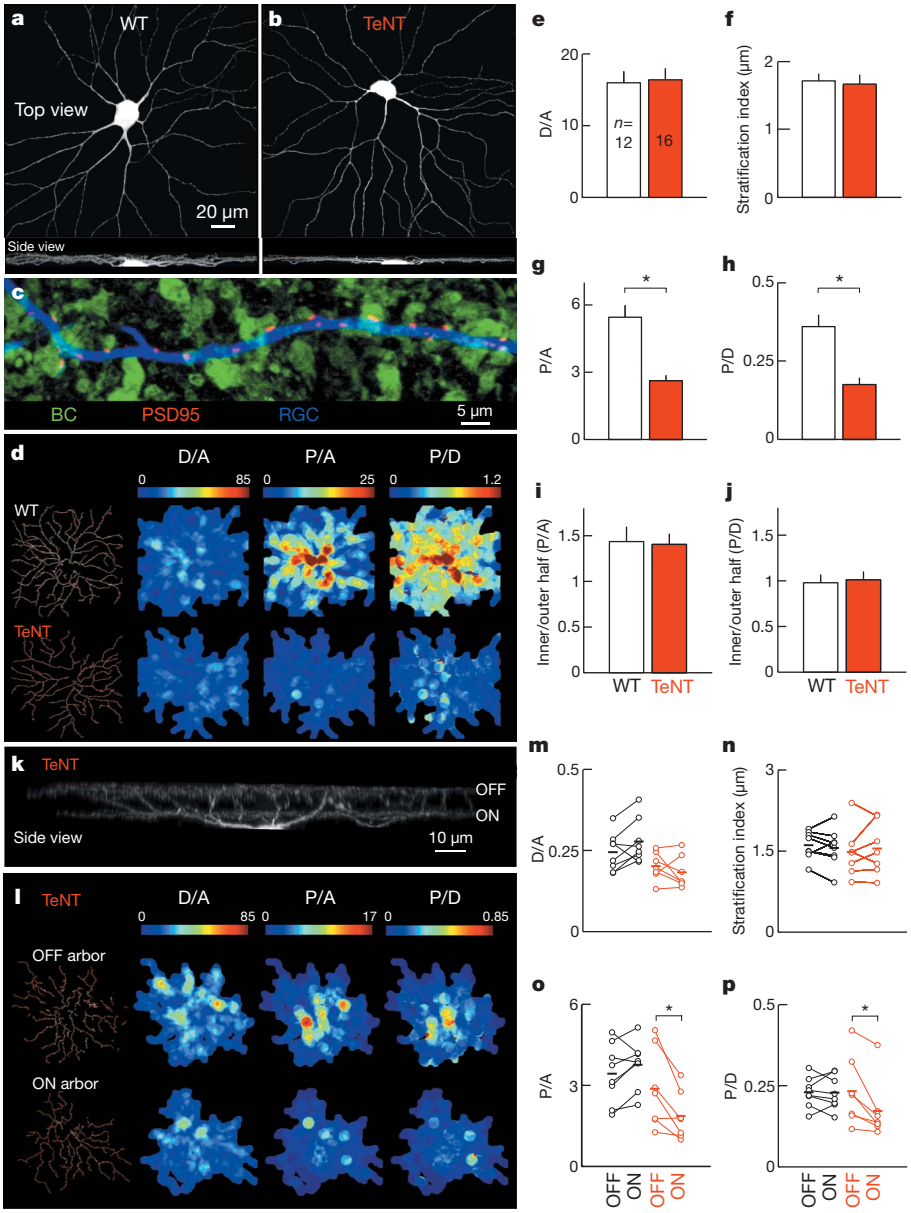

Figure 2 | Silencing ON bipolar cells reduces synapse number on RGC dendrites in an input-specific manner without changes to laminar targeting or branching. **a**, **b**, Large ON RGCs (tdTomato, postnatal day 21). **c**, RGC dendrite (tdTomato) in a TeNT retina (postnatal day 21) illustrating the localization of PSD95–CFP puncta to bipolar cell (BC, YFP) contacts (see also Supplementary Movie 1 and Supplementary Fig. 4). **d**, Maps of dendritic and glutamatergic postsynaptic densities for representative postnatal day 21 ON RGCs. **e**–**j**, Mean (±s.e.m.) RGC dendritic density (**e**, D/A) and stratification (**f**, see also Supplementary Fig. 3), areal (**g**, P/A) and linear (**h**, P/D) density of PSD95–CFP puncta, and centroperipheral gradients (**i** and **j**) of PSD95–CFP puncta across dendritic fields for large ON RGCs[13]. **k**, Bistratified ON-OFF RGC (tdTomato, postnatal day 21) in TeNT retina. **l**, Maps of dendritic and glutamatergic postsynaptic densities for OFF and ON arborization for a representative bistratified RGC in an *mGluR6-YFP/TeNT* mouse. **m**–**p**, Comparison of dendritic density (**m**, D/A) and stratification (**n**), and areal (**o**, P/A) and linear (**p**, P/D) density of PSD95–CFP puncta between the OFF and ON arbor of bistratified RGCs from wild-type (black) and *mGluR6-YFP/TeNT* (red) mice . Mean indicated by bold horizontal lines. Asterisk indicates $P < 0.01$. D/A, Dendritic length (µm) per 100 µm^2; P/A, puncta per 100 µm^2; P/D, puncta per dendritic length (µm).

formation (Fig. 4c–e and Supplementary Fig. 9) and elimination (Fig. 4f–h) events. The synaptic turnover rate was 27 ± 5.8% per day with a net increase in synapses of 11 ± 6.5% per day in wild-type mice. Surprisingly, in *mGluR6-YFP/TeNT* mice the rate of synapse formation was reduced several fold (Fig. 4i), whereas synapse elimination was indistinguishable from wild-type littermates (Fig. 4j). We verified that >90% of newly formed synapses were present in more than one time-lapse image to make sure that the reduced rate of synapse formation we report was not caused by a shortening of synapse lifetimes below our sampling interval. Moreover, the difference in the rate of synapse formation between TeNT and wild-type retinas (36 ± 13%; TeNT/wild type in per cent, Fig. 4i) was similar to the difference in synapse density increase estimated by linear regression from postnatal day 7 to 21 (23 ± 13%; TeNT/wild type in per cent, Fig. 4a). Together these results show that inhibition of glutamate release from TeNT-expressing ON bipolar cells selectively lowers the rate at which new synapses are established during development, thus accounting for the reduced density of bipolar cell–RGC synapses observed in mature *mGluR6-YFP/TeNT* mice.

The self-organization of neurons into complex circuits during development is thought to depend in part on neurotransmission. The most prominent model of activity-dependent circuit development proposes that converging inputs engage in activity-mediated competitions, the outcome of which is determined by differences in

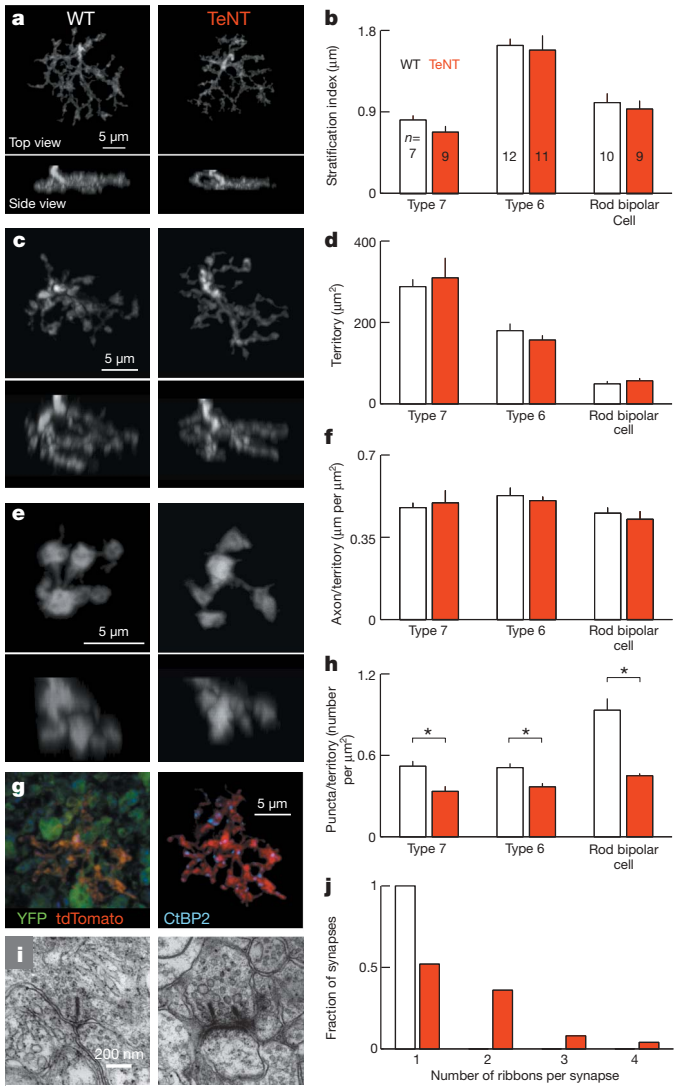

Figure 3 | Axonal morphology is normal, but multiple ribbons accumulate at fewer synapses in TeNT-expressing ON bipolar cells. **a**–**f**, Axon arborizations of representative type 7 (**a**) and type 6 (**c**) ON cone bipolar cells, and rod bipolar cells (**e**) labelled in an *mGluR6-tdTomato* mouse in wild-type (left) or *mGluR6-YFP/TeNT* (right) background at postnatal day 21. TdTomato signal was used to mask arborizations of single bipolar cells. Summary data (mean + s.e.m.) comparing stratification (**b**), lateral territories (**d**) and axonal density (**f**) between wild-type and *mGluR6-YFP/TeNT* background. **g**, Synapses on bipolar cell terminals labelled with anti-CtBP2. TdTomato signal shown in *mGluR6-YFP/TeNT* background (left) was used as a mask to isolate ribbon synapses of an individual axonal arbor (right). **h**, Mean (+s.e.m.) density of synapses for the different bipolar cell types. Asterisk indicates $P < 0.01$. **i**, Electron micrographs of ON bipolar cell ribbon synapses of wild-type (right) and *mGluR6-YFP/TeNT* (left) littermates at postnatal day 21. **j**, Histogram of the number of ribbons per synapse for wild-type (white, $n = 25$) and *mGluR6-YFP/TeNT* (red, $n = 25$) mice.

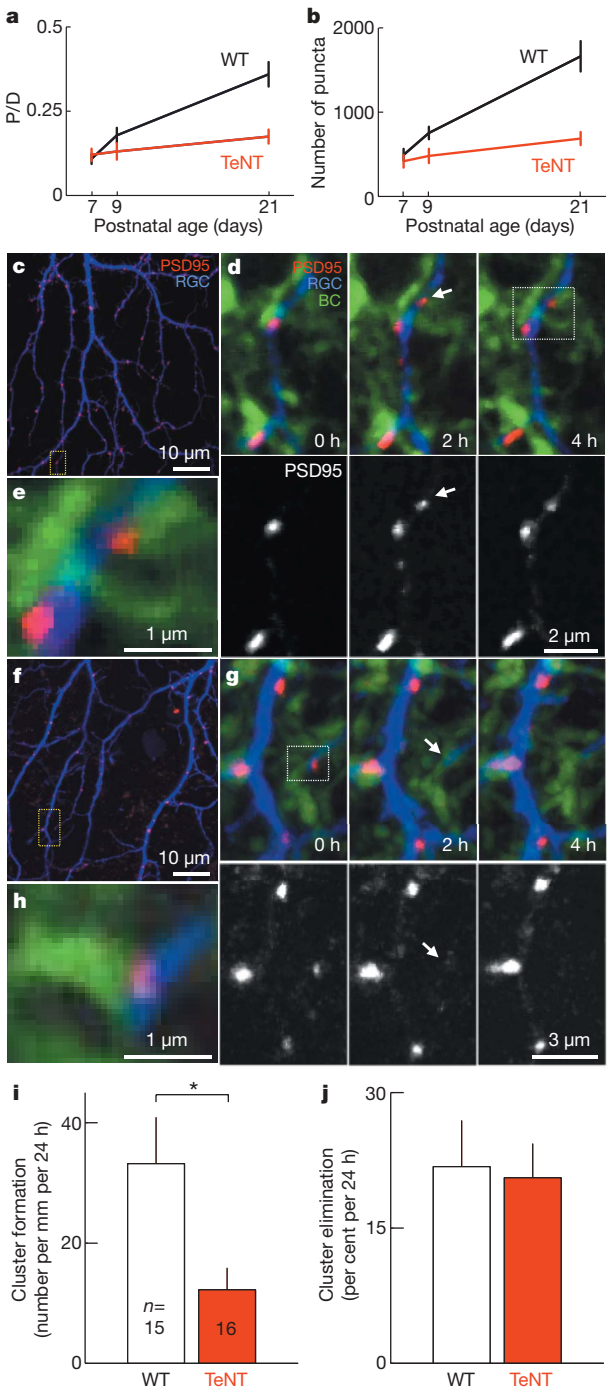

Figure 4 | Transmitter release regulates synapse formation but not elimination, causing a gradual divergence of synaptic development between wild-type and *mGluR6-YFP/TeNT* mice. **a**, **b**, Developmental increase in density (**a**) and number (**b**) of PSD95–CFP puncta on ON RGCs (5–16 cells per time point and genotype). **c**, First image of a time-lapse series of a postnatal day 9 RGC labelled with tdTomato (blue) and glutamatergic postsynaptic densities labelled with PSD95–CFP (red). **d**, Time series of the region indicated by a yellow box in **c** in which a PSD95 cluster forms (arrow). YFP expression in bipolar cells is shown in green. The PSD95–CFP channel is shown in the lower panels. **e**, Higher magnification of a single plane of the region indicated by the white box in **d** showing that the new punctum formed at an apposition of bipolar cell axon and RGC dendrite. **f**–**h**, analogous to **c**–**e** for loss of a PSD95 cluster. **i**, **j**, Summary data (mean ± s.e.m.) for the rate of PSD95–CFP cluster formation (**i**) and elimination (**j**). Asterisk indicates $P < 0.05$.

synapse elimination[1,2]. This is supported by studies of the neuromuscular junction. During development, each neuromuscular junction receives convergent innervation from multiple axons of which all but one are eventually retracted. When transmitter release from a subset of these axons is inhibited, the outcome of competition is biased towards removal of silenced axons[22,23]. In contrast, studies of RGC axons in the zebrafish tectum showed that activity could regulate branch addition rather than retraction[24], suggesting that different rules might apply in different circuits. In this study, we modified synaptic activity directly while imaging synaptic dynamics in the developing retina. In doing so we find that during the assembly of retinal circuits, glutamate release regulates the formation but not elimination of synapses between bipolar cells and RGCs. In addition, we find that rather than engaging in competition, the axons of ON

and OFF bipolar cells refine their connectivity with RGCs independent of one another, even when they converge stably onto a single postsynaptic cell. Finally, neurotransmission seems to selectively affect synaptic but not axonal or dendritic, development in this system. Which factors determine the different rules that seem to guide activity-dependent development of different neural circuits? Part of the answer might be found in the distinct architectures of early neural circuits that are set up before neurotransmission. Accordingly, the early spatial separation of ON and OFF bipolar cell axons in the inner plexiform layer might serve to constrain the role of activity in synaptic remodelling. It is tempting to speculate that laminar circuit architecture throughout the nervous system[25] might similarly serve to limit activity-dependent competition between parallel circuits that process distinct information, while allowing activity to fine-tune wiring within each information channel.

METHODS SUMMARY

Transgenic mice. We generated two transgenic mouse lines. In one (*mGluR6-YFP/TeNT*) a ~9-kb fragment of the *mGluR6* promoter was used to express yellow fluorescent protein (YFP) and the light chain of tetanus toxin (TeNT) selectively in retinal ON bipolar cells. In the other (*mGluR6-tdTomato*) the ~9-kb *mGluR6* promoter fragment drove expression of the red fluorescent protein tandem dimer Tomato (tdTomato).

Immunohistochemistry. Paraformaldehyde (4%)-fixed retinal flat-mount preparations or vibratome slices were labelled by standard immunohistochemistry procedures.

Electrophysiology. We performed whole-cell patch-clamp recordings from RGCs in retinal flat-mount preparations to analyse spontaneous excitatory synaptic transmission and used multi-electrode array recordings to characterize light responses during white noise presentation from an organic light-emitting display (OLED).

Imaging and analysis. Images of fixed tissue were acquired on an Olympus FV1000 confocal microscope using a 1.35 NA ×60 oil objective. Time-lapse imaging experiments on retinas of *mGluR6-YFP/TeNT* mice and wild-type littermates were performed in parallel on an Olympus FV1000 confocal microscope (*mGluR6-YFP/TeNT*) and either an Olympus FV300 confocal microscope or a custom-built two-photon microscope (wild type) using 1.1 NA ×60 water objectives. Image stacks were analysed using Amira (Mercury Computer System), Imaris (Bitplane) and custom software written in MATLAB (The Mathworks).

Electron microscopy. Retinas were fixed using standard electron microscopy fixation techniques, cut into pieces and en bloc-stained in uranyl acetate. Thin sections were cut and stained with Reynolds lead citrate.

Full Methods and any associated references are available in the online version of the paper at www.nature.com/nature.

Received 13 April; accepted 23 June 2009.

1. Wong, R. O. L. & Lichtman, J. W. in *Fundamental Neuroscience* 2nd edn (eds Squire, L. R. *et al.*) Ch. 20, 533–554 (Academic Press, 2002).
2. Miller, K. D. Synaptic economics: competition and cooperation in synaptic plasticity. *Neuron* **17,** 371–374 (1996).
3. Masland, R. H. The fundamental plan of the retina. *Nature Neurosci.* **4,** 877–886 (2001).
4. Wassle, H. Parallel processing in the mammalian retina. *Nature Rev. Neurosci.* **5,** 747–757 (2004).
5. Ueda, Y., Iwakabe, H., Masu, M., Suzuki, M. & Nakanishi, S. The mGluR6 5′ upstream transgene sequence directs a cell-specific and developmentally regulated expression in retinal rod and ON-type cone bipolar cells. *J. Neurosci.* **17,** 3014–3023 (1997).
6. Schiavo, G. *et al.* Tetanus and botulinum-B neurotoxins block neurotransmitter release by proteolytic cleavage of synaptobrevin. *Nature* **359,** 832–835 (1992).
7. Harms, K. J. & Craig, A. M. Synapse composition and organization following chronic activity blockade in cultured hippocampal neurons. *J. Comp. Neurol.* **490,** 72–84 (2005).
8. Chichilnisky, E. J. A simple white noise analysis of neuronal light responses. *Network* **12,** 199–213 (2001).
9. Maslim, J., Webster, M. & Stone, J. Stages in the structural differentiation of retinal ganglion cells. *J. Comp. Neurol.* **254,** 382–402 (1986).
10. Coombs, J. L., Van Der List, D. & Chalupa, L. M. Morphological properties of mouse retinal ganglion cells during postnatal development. *J. Comp. Neurol.* **503,** 803–814 (2007).
11. Wang, G. Y., Liets, L. C. & Chalupa, L. M. Unique functional properties of On and Off pathways in the developing mammalian retina. *J. Neurosci.* **21,** 4310–4317 (2001).
12. Nelson, R., Famiglietti, E. V. Jr & Kolb, H. Intracellular staining reveals different levels of stratification for on- and off-center ganglion cells in cat retina. *J. Neurophysiol.* **41,** 472–483 (1978).
13. Morgan, J. L., Schubert, T. & Wong, R. O. L. Developmental patterning of glutamatergic synapses onto retinal ganglion cells. *Neural Develop.* **3,** 8 (2008).
14. Morgan, J. L., Dhingra, A., Vardi, N. & Wong, R. O. L. Axons and dendrites originate from neuroepithelial-like processes of retinal bipolar cells. *Nature Neurosci.* **9,** 85–92 (2006).
15. Ghosh, K. K., Bujan, S., Haverkamp, S., Feigenspan, A. & Wassle, H. Types of bipolar cells in the mouse retina. *J. Comp. Neurol.* **469,** 70–82 (2004).
16. Sterling, P. & Matthews, G. Structure and function of ribbon synapses. *Trends Neurosci.* **28,** 20–29 (2005).
17. Regus-Leidig, H., Tom Dieck, S., Specht, D., Meyer, L. & Brandstatter, J. H. Early steps in the assembly of photoreceptor ribbon synapses in the mouse retina: the involvement of precursor spheres. *J. Comp. Neurol.* **512,** 814–824 (2009).
18. Zhai, R. G. *et al.* Assembling the presynaptic active zone: a characterization of an active one precursor vesicle. *Neuron* **29,** 131–143 (2001).
19. Johnson, J. *et al.* Vesicular neurotransmitter transporter expression in developing postnatal rodent retina: GABA and glycine precede glutamate. *J. Neurosci.* **23,** 518–529 (2003).
20. Okabe, S., Miwa, A. & Okado, H. Spine formation and correlated assembly of presynaptic and postsynaptic molecules. *J. Neurosci.* **21,** 6105–6114 (2001).
21. Niell, C. M., Meyer, M. P. & Smith, S. J. *In vivo* imaging of synapse formation on a growing dendritic arbor. *Nature Neurosci.* **7,** 254–260 (2004).
22. Buffelli, M. *et al.* Genetic evidence that relative synaptic efficacy biases the outcome of synaptic competition. *Nature* **424,** 430–434 (2003).
23. Kasthuri, N. & Lichtman, J. W. The role of neuronal identity in synaptic competition. *Nature* **424,** 426–430 (2003).
24. Hua, J. Y., Smear, M. C., Baier, H. & Smith, S. J. Regulation of axon growth *in vivo* by activity-based competition. *Nature* **434,** 1022–1026 (2005).
25. Sanes, J. R. & Yamagata, M. Formation of lamina-specific synaptic connections. *Curr. Opin. Neurobiol.* **9,** 79–87 (1999).

Supplementary Information is linked to the online version of the paper at www.nature.com/nature.

Acknowledgements We are grateful to J. Sanes and R. W. Burgess for TeNT–CFP, S. Naganishi for the *mGluR6* promoter fragment, A. M. Craig for PSD95–CFP and R. Y. Tsien for tdTomato. We thank F. Soto, L. Godinho, A. Lewis, F. Dunn and T. Misgeld for comments on the manuscript. This work was supported by the National Institutes of Health (R.O.L.W., EY10699, J.L.M. T32 EY07031), the McDonnell Foundation at Washington University (R.O.L.W.), National Eye Institute core grant (E.D.P., EY01730) and the Deutsche Forschungsgemeinschaft (D.K., KE 1466/1-1).

Author Contributions D.K. and R.O.L.W. conceived the experiments. D.K. and R.M.L. generated transgenic constructs. D.K. performed and analysed patch-clamp and multi-electrode array recordings, and imaging experiments on fixed tissue. D.K. and J.L.M. performed and analysed live imaging experiments. D.K., E.D.P. and R.O.L.W. carried out the ultrastructural analysis. D.K. and R.O.L.W. wrote the paper.

Author Information Reprints and permissions information is available at www.nature.com/reprints. Correspondence and requests for materials should be addressed to D.K. (KerschensteinerD@vision.wustl.edu) or R.O.L.W. (wongr2@u.washington.edu).

METHODS

Transgenic mice. The following transgenic constructs were assembled using standard cloning techniques. *mGluR6-loxP-YFPstop-loxP-TeNT-CFP*: a 9.5-kb fragment of the *mGluR6* promoter[5] (gift of S. Nakanishi) was placed upstream of a 2.5-kb *YFPstop* cassette which was flanked by two *loxP* sites. The *YFPstop* cassette contained the coding sequence of enhanced yellow fluorescent protein followed by the 3′ UTR and transcription stop site of the rabbit β-globin gene. A 2.3-kb *TeNT–CFP* cassette encoding a carboxy-terminal fusion of enhanced cyan fluorescent protein to the light chain of tetanus toxin (TeNT–CFP, gift of R.W. Burgess and J.R. Sanes) was inserted 3′ of the second *loxP* site. *mGluR6-tdTomato*: the 9.5-kb *mGluR6* promoter fragment was positioned upstream of the coding sequence of the red fluorescent protein tdTomato[26]. Linearized constructs were injected into pronuclei of murine oocytes to generate transgenic mouse lines. We refer to these lines as *mGluR6-YFP/TeNT* and *mGluR6-tdTomato* throughout the text. PCR genotyping was performed using primers to enhanced yellow fluorescent protein (5′-GACTTCTTCAAGTCCGCCATG CC-3′ and 5′-GTGATCCCGGCGGCGGTCACG-3′) and tdTomato (5′-CTCC TCCGAGGACAACAACATGG and 5′-CTTGGTCACCTTCAGCTTGGCGG-3′).

We initially crossed *mGluR6-YFP/TeNT* mice to *Pax6$_\alpha$-cre* mice[27] to excise the *YFPstop* cassette and allow expression of TeNT–CFP. Although retinal ON bipolar cells in mice carrying both transgenes showed varying mixtures of YFP and CFP fluorescence, the TeNT substrate synaptobrevin/VAMP2 was cleaved uniformly in these cells (data not shown). To our surprise, this was also true for ON bipolar cells in the dorso-ventral wedge of the retina which in *Pax6$_\alpha$-cre* mice do not express Cre recombinase[27]. We next verified that VAMP2 was cleaved even in ON bipolar cells of *mGluR6-YFP/TeNT* mice that had not been crossed to *Pax6$_\alpha$-cre* mice (Fig. 1c–h). In addition, we could detect dim CFP fluorescence in these cells (data not shown). Weak expression of TeNT–CFP in these mice could be caused by occasional transcription past the *YFPstop* cassette or spontaneous recombination and excision of this cassette in one or a few of the copies of the transgene array. Because weak TeNT–CFP expression was sufficient to block release from ON bipolar cells (Fig. 1i, j), we used *mGluR6-YFP/TeNT* mice without crossing to *Pax6$_\alpha$-cre* mice throughout this study. We observed some variation in the number of bipolar cells expressing the transgene even among littermates. In particular, some mice showed patchy expression patterns across the retina that were most likely due to transgene-induced gene silencing. For the present study we excluded those retinas. To do so we monitored YFP expression pattern in both electrophysiological and imaging experiments.

Tissue preparation. All experiments were carried out following the guidelines of the Institutional Animal Care and Use Committee at the University of Washington and in compliance with the National Institute of Health Guide for the Care and Use of Laboratory Animals. Mice, deeply anaesthetized with isoflurane, were decapitated and enucleated. Each cornea was punctured with a 30 gauge needle and the eyes placed in cold oxygenated mouse artificial cerebrospinal fluid (mACSF) containing 119 mM NaCl, 2.5 mM KCl, 2.5 mM $CaCl_2$, 1.3 mM $MgCl_2$, 1 mM NaH_2PO_4, 11 mM glucose and 20 mM HEPES. mACSF was brought to pH 7.35 with NaOH. For vibratome sections, the lens and vitreous were removed and the remaining eyecup fixed for 30 min in 4% paraformaldehyde in mACSF. For electron microscopy, eyecups were placed in 2% glutaraldehyde and 2% paraformaldehyde in 0.1 M sodium cacodylate (pH 7.4) for 10 min. For flat-mount preparation, the retina was isolated and mounted ganglion cell side up on membrane discs (Millipore) before fixation (30 min in 4% paraformaldehyde in mACSF), biolistic transfection or patch-clamp electrophysiology.

Immunohistochemistry. Fixed retinal flat mounts or vibratome slices were labelled with the antibodies anti-CaBP5 (1:1,000, gift of F. Haessler and K. Palczewski), anti-VAMP2 (1:1,000, Synaptic Systems), anti-CtBP2 (1:1,000, BD Bioscience Pharmingen) and anti-GluR2/3 (1:1,000, Upstate). Secondary antibodies were Alexa 568 or Alexa 633 conjugates (1:1,000, Invitrogen).

Biolistic transfection. Gold particles (12.5 mg, 1.0 or 1.6 μm diameter, Bio-Rad) were coated with cytomegalovirus-promoter-driven PSD95–CFP (10 μg) and tdTomato (20 μg) plasmids and delivered to RGCs in a flat-mount preparation using a Helios gene gun (~40 psi, Bio-Rad). Transfected retinas were incubated in mACSF in a humid oxygenated chamber at ~33 °C for 18–24 h, and transferred to a live imaging chamber or fixed for 30 min in 4% paraformaldehyde in mACSF.

Confocal imaging of fixed tissue and analysis. RGC image stacks were acquired on an Olympus FV1000 laser scanning confocal microscope using a 1.35 NA ×60 oil objective at a voxel size of 0.103 × 0.103 × 0.3 μm (*x-y-z*) except for the data set in Supplementary Fig. 3 which was imaged using a 0.8 NA ×25 oil objective at a voxel size of 0.247 × 0.247 × 0.5 μm (*x-y-z*). Voxel size for image stacks of bipolar cell axons acquired using a 1.35 NA ×60 oil objective was 0.041 × 0.041 × 0.3 μm (*x-y-z*).

Morphometric analysis of RGC dendrites and mapping of excitatory synapses were carried out largely as described previously[13]. Dendritic territories were defined by dilating the dendritic skeleton with a 10 μm diameter disk. Within the dendritic territory of each cell, dendritic length (μm) per 100 μm^2 (D/A), puncta per 100 μm^2 (P/A) and puncta per dendritic length (μm; P/D) were measured. The stratification index was defined differently from the previous study[13], as the s.d. of *z*-positions of the ~0.5 μm long segments that form the dendritic skeleton. To reduce the influence of irregularities in the tissue, the average *z*-position used in the calculation of the s.d. was updated for each segment as the average *z*-position of segments within 30 μm in *x-y* of the current segment. In order to compare distributions only across the stratified arborizations, the analysis excluded dendrites within 10 μm from the cell body.

To isolate axonal arborizations of single bipolar cells, *mGluR6-YFP/TeNT* mice were crossed to a line of *mGluR6-tdTomato* mice in which ON bipolar cells were labelled at a low density. Presynaptic release sites were labelled with antibodies against the ribbon protein CtBP2. The tdTomato signal was used to mask (Amira, Mercury Computer Systems) parts of the image stack representing a single bipolar cell. To measure arbor length, axons were skeletonized based on the binary mask of the tdTomato signal using an algorithm similar to the one used for RGC dendrites[13]. Arbor stratification was measured as above. Axonal territories were defined by the smallest convex polygon encompassing the arbor in a *z*-projection. To automate counting of synapses on bipolar cell axons, the masked CtBP2 image was median-filtered and thresholded at every other grey value from 255 to 0. For each threshold, objects containing <6 or >343 connected voxels were removed. The position of the peak intensity of each remaining object was noted in a binary peak map. Within the iterative thresholding loop a summary image was accumulated in which the intensity of each voxel signified the number of times it passed threshold when associated with an object of acceptable size (6–343 voxels). In the next step, objects of connected voxels in this summary image were identified and split into multiple objects if they were associated with more than one entry in the peak map. These objects will be referred to as potential synapses. The voxels associated with a potential synapse were defined as all voxels of the respective object whose intensity exceeded half the intensity of its peak. For each potential synapse two parameters were calculated: strength and surprise. Strength was defined as the summed intensity across all voxels of one synapse in the summary image divided by their average brightness in the median-filtered CtBP2 image. To calculate surprise, we first determined the expected intensity of the CtBP2 channel given the value of the tdTomato channel from linear regression of both channels at voxels outside potential synapses. Next the difference between the observed brightness in the CtBP2 channel and its expected brightness for each voxel of a potential synapse was calculated and normalized by the expected brightness. The surprise of a potential synapse was defined as the average of this normalized difference for the brightest half of its voxels. For each bipolar cell, all potential synapses were depicted in a coordinate system of strength and surprise, and the cluster of acceptable synapses selected via a graphical user interface. For each cell this selection was verified by overlaying the position of acceptable synapses on the CtBP2 image. We confirmed that this procedure correctly identified >90% of the synaptic puncta identified by eye on a randomly chosen subset of cells. All scripts for customized image analysis were written in MATLAB (The MathWorks).

Confocal and two-photon live imaging and analysis. Time-lapse imaging experiments on retinas of *mGluR6-YFP/TeNT* mice and wild-type littermates (~postnatal day 9) were performed using an Olympus FV1000 confocal microscope (*mGluR6-YFP/TeNT*, three-colour images) and either an Olympus FV300 confocal or a custom-built two-photon microscope (wild type, two-colour images) using 1.1 NA ×60 water objectives. Flat-mounted retinas were continuously perfused with oxygenated mACSF and heated to 31–33 °C. Image stacks were acquired every 2 h for up to 14 h. Voxel size was between 0.103 × 0.103 × 0.3 μm (*x-y-z*) and 0.115 × 0.115 × 0.3 μm (*x-y-z*). For analysis image stacks were median-filtered to reduce photomultiplier noise. PSD95–CFP puncta were identified in image stacks by eye and manually tracked through time series. The synaptic turnover rate was calculated as $(N_{\text{formations}} + N_{\text{eliminations}})/(2 \times N_{\text{total}})$, where $N_{\text{formations}}$ is the number of new synapses, $N_{\text{eliminations}}$ is the number of lost synapses and N_{total} is the sum of all synapses. Dendrites were reconstructed and their length measured using Imaris (Bitplane). To avoid biasing measurement of synapse formation and stability by differences in the synapse number at the beginning of the imaging experiment, the rate of formation was normalized by the length of the dendrite and the rate of synapse elimination was expressed as the percentage of puncta that were lost.

Electron microscopy. After the initial fixation (described under Tissue preparation) retinas were cut into ~1 mm^2 pieces and left in fixative overnight at 4 °C. The pieces of retina were then washed four times for 5 min in sodium cacodylate buffer and post-fixed for 45 min in buffered 1% osmium tetroxide. Next, the

tissue was washed four times for 5 min in dH_2O, en bloc-stained in 1% aqueous uranyl acetate, and washed twice again in dH_2O before being dehydrated through a series of ethanol and propylene oxide and embedded in Epon Araldite resin. Thin sections (70 nm) were cut, placed on Formvar-coated slot grids and stained with Reynolds lead citrate.

Patch-clamp recording. Retinal flat mounts were prepared as described above and bathed in bicarbonate-buffered mACSF containing 125 mM NaCl, 2.5 mM KCl, 2 mM $CaCl_2$, 1 mM $MgCl_2$, 1.25 mM NaH_2PO_4, 11 mM glucose and 26 mM $NaHCO_3$ (equilibrated with 95% O_2 and 5% CO_2). Whole-cell recordings were performed with electrodes (4–8 MΩ) filled with 120 mM Cs-gluconate, 1 mM $CaCl_2$, 1 mM $MgCl_2$, 10 mM Na-HEPES, 11 mM EGTA, 10 mM TEA-Cl and 2 mM QX314 (pH 7.2 adjusted with CsOH). Data were acquired using an Axopatch 200B amplifier (Molecular Devices), low-pass filtered at 2 kHz and digitized at 5 kHz. sEPSC were recorded at –60 mV, the reversal potential of chloride currents in our recording conditions. Area and amplitude thresholds (Mini Analysis, Synaptosoft) were optimized to detect >90% of the events identified by eye in excerpts from each recording. For overlapping events, the baseline for amplitude measurement of each event was estimated from exponential decay extrapolation of the previous event. RGCs were classified as ON or OFF based on their stratification pattern that was visualized by including sulforhodamine B (0.005%) in the recording pipette.

Multi-electrode array recording and visual stimulation. Retinas were isolated as described above, transferred to a chamber containing the array (HD MEA, Multi Channel Systems), floated onto the electrodes RGC-side down and held in place by a transparent tissue culture membrane (Corning) and a platinum ring. During recordings the tissue was perfused with bicarbonate-buffered mACSF equilibrated with 95% O_2 and 5% CO_2. The temperature of the bath was maintained at 31–33 °C. Signals were band-pass filtered between 0.1 and 3 kHz and digitized at 10 kHz. Spikes were detected by negative thresholds and sorted into trains representing the activity of single cells (Offline Sorter, Plexon). Only cells for which <1% of interspike intervals were <2 ms were used in our analysis. Duplicates, that is, cells recorded on multiple electrodes were identified by cross-correlation of spike trains, and only the train with the highest number of spikes was kept. Stimuli composed of a lattice of squares, each flickering randomly and independently at 25 Hz, were presented on a monochrome yellow organic light-emitting diode microdisplay (OLED, eMagin) at a mean equivalent intensity of $\sim 10^4$ photoisomerizations per middle-wavelength-sensitive cone per second. Each square had a side length of 50 μm on the retina. Response properties of RGCs were characterized by the spike-triggered average (STA) stimulus calculated from reverse correlation of its spike train to the stimulus[8,28].

Statistics. We used either Wilcoxon–Mann–Whitney rank sum or, in case of paired samples, Wilcoxon signed-rank tests to assess statistical significance of differences between groups.

26. Shaner, N. C. *et al.* Improved monomeric red, orange and yellow fluorescent proteins derived from *Discosoma* sp. red fluorescent protein. *Nature Biotechnol.* **22**, 1567–1572 (2004).
27. Marquardt, T. *et al.* Pax6 is required for the multipotent state of retinal progenitor cells. *Cell* **105**, 43–55 (2001).
28. Kerschensteiner, D. *et al.* Genetic control of circuit function: *Vsx1* and *Irx5* transcription factors regulate contrast adaptation in the mouse retina. *J. Neurosci.* **28**, 2342–2352 (2008).